

Boise State University

ScholarWorks

---

Electrical and Computer Engineering Faculty  
Publications and Presentations

Department of Electrical and Computer  
Engineering

---

8-1-2022

## Ultra-Compact Hybrid Silicon: Chalcogenide Waveguide Temperature Sensor

Bahareh Badamchi  
*Boise State University*

Wei-Che Hsu  
*Oregon State University*

Al-Amin Ahmed Simon  
*Boise State University*

Zong Yin Chi  
*Boise State University*

Jacob Manzi  
*Boise State University*

*See next page for additional authors*

---

**Authors**

Bahareh Badamchi, Wei-Che Hsu, Al-Amin Ahmed Simon, Zong Yin Chi, Jacob Manzi, Maria Mitkova, Alan X. Wang, and Harish Subbaraman



# Ultra-compact hybrid silicon:chalcogenide waveguide temperature sensor

BAHAREH BADAMCHI,<sup>1</sup>  WEI-CHE HSU,<sup>2</sup> AL-AMIN AHMED SIMON,<sup>1</sup> ZONG YIN CHI,<sup>1</sup> JACOB MANZI,<sup>1</sup> MARIA MITKOVA,<sup>1</sup> ALAN X. WANG,<sup>2</sup> AND HARISH SUBBARAMAN<sup>1,\*</sup>

<sup>1</sup>Department of Electrical and Computer Engineering, Boise State University, Boise, ID 83725, USA

<sup>2</sup>School of Electrical Engineering and Computer Science, Oregon State University, Corvallis, OR 97331, USA

\*harishsubbaraman@boisestate.edu

**Abstract:** We demonstrate a real-time, reusable, and reversible integrated optical sensor for temperature monitoring within harsh environments. The sensor architecture combines the phase change property of chalcogenide glasses (ChG) with the high-density integration advantages of high index silicon waveguides. To demonstrate sensor feasibility, ChG composition Ge<sub>40</sub>S<sub>60</sub>, which is characterized by a sharp phase transition from amorphous to crystalline phase around 415 °C, is deposited over a 50 μm section of a single mode optical waveguide. The phase transition changes the behavior of Ge<sub>40</sub>S<sub>60</sub> from a low loss to high loss material, thus significantly affecting the hybrid waveguide loss around the phase transition temperature. A transmission power drop of over 40dB in the crystalline phase compared to the amorphous phase is experimentally measured. Moreover, we recover the amorphous phase through the application of an electrical pulse, thus showing the reversible nature of our compact temperature sensor. Through integrating multiple compositions of ChG with well-defined phases transition temperatures over a silicon waveguide array, it is possible to determine, in real-time, the temperature evolution within a harsh environment, such as within a nuclear reactor cladding.

© 2022 Optica Publishing Group under the terms of the [Optica Open Access Publishing Agreement](#)

## 1. Introduction

In extreme environments, such as within a nuclear reactor, one of the most frequently measured physical parameters is temperature. Often, temperature change can be an indicator of physical changes occurring in other parameters of interest. To observe material performance (microstructure, chemistry, mechanical, and other property changes with the changing conditions) while exposed to the reactor environment and to prevent disasters caused by structural failure due to high temperature, real-time and accurate sensing devices are required [1–3]. Precise temperature monitoring of the cladding of each nuclear reactor is critical for its safety, stability, proper functionality, and efficient operation over the long term operational lifetime [4–6]. The desire to reduce sensor ownership cost and overcome the limitation of traditional (electrical) temperature sensors led to considerable interest in deploying photonic temperature sensors within nuclear power plants as well as within high energy physics experiments [7–12].

Chalcogenide glasses (ChGs) are inorganic amorphous compounds containing one or more of the chalcogen elements (group 6a of the periodic table), such as Sulphur, Selenium, and Tellurium but excluding Oxygen, covalently bonded to other elements such as As, Ge, Sb, Ga, Si, or P. The chalcogen elements with other metal or nonmetal elements exhibit unique optical nonlinear and mid-infrared properties such as wide infrared 0.8-1.6 μm wavelength transparency windows. ChGs, owing to the lack of order in their structure and the presence of lone pair p-shell electrons, contain a high number of defects [13,14]. These defects combined with the defects occurring as a result of irradiation [15] become populated in very close proximity due to which their recombination occurs rapidly, leading to radiation hardness behavior of the material. ChGs are

easy to synthesize in bulk and thin film forms and their compositional flexibility allows tuning of optical properties, such as refractive index, making them good candidates for infrared photonics. These glasses demonstrate ultra-fast crystallization rates and large optical contrast between their amorphous (disordered) and crystalline (ordered) phase's properties, making them good candidates for infrared phase change photonic applications [16–21]. ChGs undergo a reversible solid-solid phase transition and become crystalline at a certain well-documented temperature which is called crystallization temperature ( $T_c$ ). There are three significant temperatures in ChGs: (1) glass transition temperature ( $T_g$ ), (2) crystallization onset temperature ( $T_o$ ), and (3) glass peak crystallization temperature ( $T_c$ ). The glass transition temperature ( $T_g$ ) is the main characteristic of a glass. It is related to the onset of fluidity. The ChG can be re-converted to its initial amorphous condition through thermodynamic conditions by applying short optical [22] or electrical pulses with relatively low energies as low as femtojoules [20,21]. Assuming ideal behavior from ChGs: below the crystallization temperature, ChGs demonstrate good dielectric behavior. When the temperature of the ambient is above the crystallization transition temperature of ChG, the material crystallizes and exhibits excellent conductive characteristics.

In this paper, through combining the unique temperature-dependent material properties of  $\text{Ge}_{40}\text{S}_{60}$  glass with compact silicon waveguides, we demonstrate a reversible, real-time temperature sensor capable of operating at temperatures up to 415 °C, although with specific adjustment of the composition of the ChG material, these sensors can become useful for metallic or ceramic Sodium-cooled Fast Reactors (SFRs) where the cladding temperature can reach 590 °C.

Ge-Se and Ge-S glasses are two compositions which have glass temperature ( $T_g$ ,  $T_o$ , and  $T_c$ ) in this range [23]. Using an array of ChG coated waveguides [24], wherein each waveguide is coated with a different ChG composition, will allow for the real-time monitoring of temperature inside extreme environments, thus mapping out the temperature profile.

## 2. Sensor design

The device architecture of the sensor, proposed in this work is presented in Fig. 1. Although we used commercially available silicon-on-insulator (SOI) wafer with a 0.22  $\mu\text{m}$  thick device layer and a 3  $\mu\text{m}$  buried oxide layer, in order to save computation time, all of the simulations were performed assuming a 2  $\mu\text{m}$  BOX. No notable differences in device performance were observed in using the 2  $\mu\text{m}$  versus 3  $\mu\text{m}$  BOX in our simulations. The refractive indices of  $\text{SiO}_2$  and Si used in simulations are  $n_{\text{SiO}_2} = 1.45$  and  $n_{\text{Si}} = 3.47$ , respectively at an operating wavelength of 1550 nm [25]. A short section,  $L$ , of the Si waveguide is covered by  $\text{Ge}_{40}\text{S}_{60}$  glass. A thin  $\text{SiO}_2$  over the ChG acts as a passivation layer. For the device simulations, previously reported measured values of  $\text{Ge}_{40}\text{S}_{60}$  refractive index and extinction coefficient characteristic for the amorphous and crystalline phases are used ( $n_{\text{amor}} = 2.6768 + i0$  and  $n_{\text{crys}} = 2.72309 + i0.17664$ ) [24]. The modal properties of the Si:ChG waveguide in the amorphous and crystalline phases of  $\text{Ge}_{40}\text{S}_{60}$  glass are investigated using Eigenmode Expansion Method software from PhotonDesign, which utilizes fully vectorial finite-difference mode solver and beam propagation method. Through performing a systematic scan of ChG layer width ( $W_{\text{ChG}}$ ) and ChG layer height ( $h_{\text{ChG}}$ ) parameters, we determined the optimum design parameters for minimum  $W_{\text{ChG}}$  and  $h_{\text{ChG}}$ , while maximizing the extinction ratio in the transmitted power between the amorphous and crystalline phases of ChG, as shown in Table 1.

Through these simulations, we also studied the behavior of the fundamental transverse electric (TE) modes propagating along the single mode silicon waveguide in amorphous and crystalline ChG phases. In the amorphous state, when the ambient temperature is below the phase transition temperature of  $\text{Ge}_{40}\text{S}_{60}$  ( $T < T_c$ ), the glass behaves like a dielectric material with a negligible extinction coefficient ( $k \sim 0$ ). Figure 2(a) shows the cross-sectional intensity distribution (mode profile) of the TE mode in the waveguide. Figure 2(b) illustrates the intensity distribution along

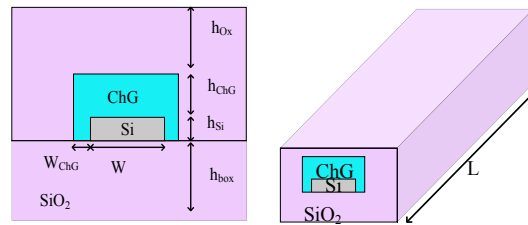


**Fig. 1.** (left) Cross section of proposed design consisting of a ChG glass covering a single mode silicon waveguide.  $W$ : silicon waveguide width;  $h_{Si}$ : silicon waveguide height;  $h_{ChG}$ : ChG film thickness;  $h_{box}$ : buried oxide layer thickness; (right) isometric view of the proposed structure. Active device length is denoted as  $L$ .

**Table 1. Optimum design parameters obtained for our proposed design.**

Parameter	Value ( $\mu\text{m}$ )	Parameter	Value ( $\mu\text{m}$ )
$W$	0.45	$h_{Ox}$	0.5
$W_{ChG}$	0.1	$L$	5
$h_{Si}$	0.22		
$h_{ChG}$	0.3		

the waveguide and the normalized output power over a compact (length up to  $5 \mu\text{m}$ ) waveguide, respectively. From Fig. 2(b), it can be seen that in the amorphous phase of  $\text{Ge}_{40}\text{Se}_{60}$ , the TE mode propagates along the waveguide with minimum loss.

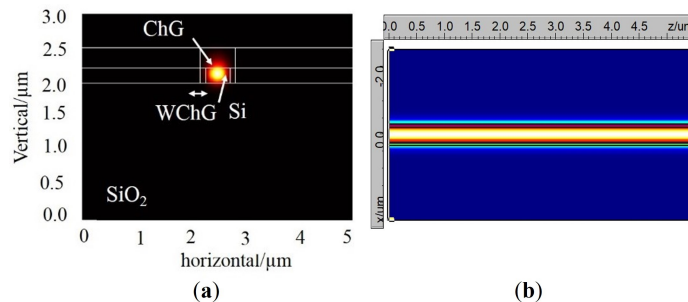


**Fig. 2.** Amorphous  $\text{Ge}_{40}\text{S}_{60}$  case: a) Intensity profile of TE mode, b) Intensity distribution along the waveguide.

As the temperature increases beyond the phase transition temperature of  $\text{Ge}_{40}\text{S}_{60}$  ( $T > T_c$ ), the material transforms into its crystalline phase and exhibits a very high extinction coefficient ( $k = 0.17664$ ) [24], which leads to a very strong absorption within ChG layer as light propagates through the waveguide, as shown in Fig. 3(b). Such an abrupt change in the transmitted power occurring around the phase transition temperature forms the basis for the operation of the studied temperature sensor. Additionally, through integrating an array of the designed waveguide with different chalcogenide glass compositions having different specific crystallization temperatures, accurate real-time temperature profile can be determined by monitoring the output powers from the array.

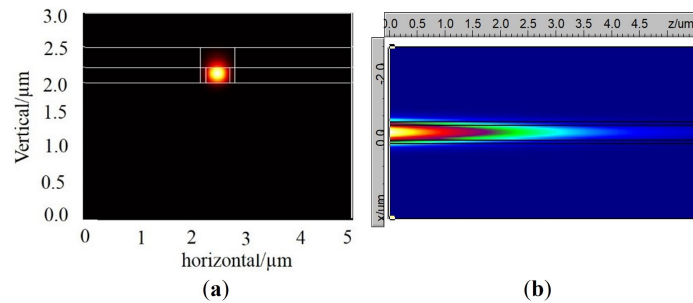


**Fig. 3.** Crystalline  $\text{Ge}_{40}\text{S}_{60}$  case: a) Intensity profile of TE mode, b) Intensity distribution along the waveguide.

### 3. Sensor fabrication

The process flow for fabricating the hybrid silicon:ChG waveguide sensors is shown in Fig. 4. The process starts with a SOI substrate (0.22  $\mu\text{m}$  silicon device layer; 3  $\mu\text{m}$  buried oxide layer (BOX); 725  $\mu\text{m}$  silicon handle substrate). After cleaning the SOI substrate using acetone and Isopropyl Alcohol (IPA), a positive e-beam resist (ZEP520A) is spin coated and e-beam lithography (EBL) is used to define the waveguide structure in the e-beam resist. Next, the defined pattern is transferred to the Si device layer using reactive ion etching (RIE). Finally, the remaining resist is removed using stripper and oxygen plasma. This completes the silicon waveguide fabrication process. As the final step, our in-house synthesized ChG is thermally evaporated through a shadow mask over a 50  $\mu\text{m}$  section of the fabricated silicon waveguide. The measured thickness of the film is  $\sim 300$  nm."

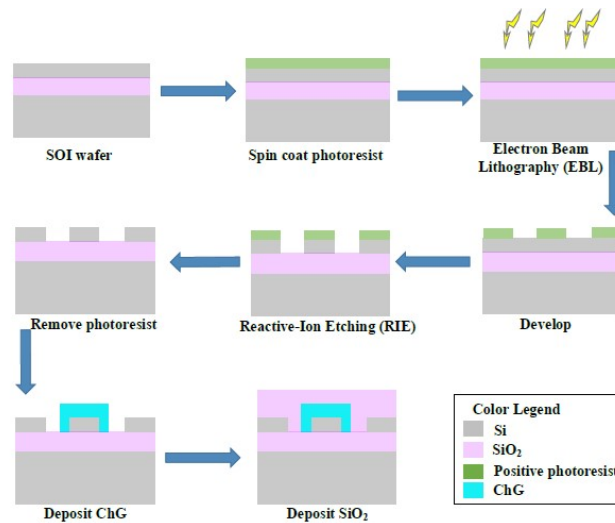


**Fig. 4.** Process flow for fabricating Silicon: ChG based hybrid waveguide temperature sensors.

The evaporation conditions were as follows:  $10^{-6}$  mbar vacuum and evaporation rate of 0.35  $\text{\AA}/\text{s}$ . A scanning electron microscope image of a waveguide covered with  $\text{Ge}_{40}\text{S}_{60}$  is displayed in Fig. 5. To demonstrate reversible operation of the sensor devices, aluminum electrodes were additionally deposited on some sample devices to facilitate electrical pulse application.

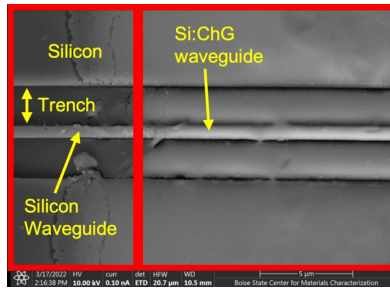


**Fig. 5.** Scanning electron microscope image of the fabricated device showing thermally evaporated chalcogenide glass covering section of the Si waveguide.

#### 4. Sensor characterization

The experimental setup to characterize the temperature performance of the fabricated device is shown in Fig. 6(a). The fabricated sensor chip is mounted on top of a programmable heating stage (INSTECH, HCS621G). Light is coupled into and out of the device using a grating coupler setup shown in Fig. 6(b). The input/output fibers are tilted at  $10^\circ$  with respect to normal to achieve the highest coupling efficiency. Initially, a red laser is coupled into the input/output fibers to aid with the alignment of the fibers with the grating couplers. Following this, 1550nm light from an external cavity laser (Santec ESL100) is coupled into the input grating coupler. The temperature of the heat stage is increased from room temperature ( $25^\circ\text{C}$ ) to  $600^\circ\text{C}$  in  $10^\circ\text{C}/\text{min}$  increments and the transmitted power obtained from the fiber coupled to the output grating coupler is monitored using an optical spectrum analyzer (Anritsu-MS9740A).

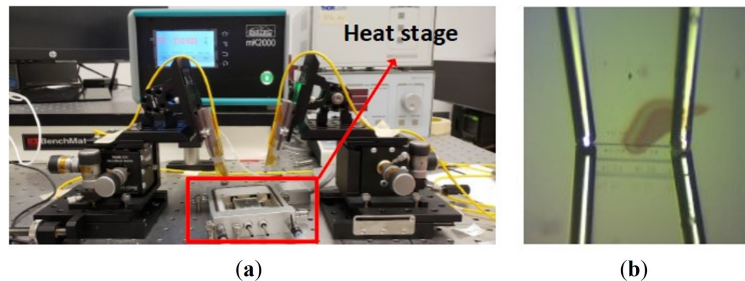


**Fig. 6.** a) Waveguide characterization setup to test the temperature response of the fabricated sensor device. The setup consists of the fabricated chip mounted on top of the heat stage within a grating coupler setup, b) close view of grating coupling region on the fabricated device.

#### 5. Results and discussion

The measured normalized transmitted power for  $\text{Ge}_{40}\text{S}_{60}$  as a function of temperature is presented in Fig. 7. It can be seen from the figure that the measured data indicates a sudden transition in power at  $415^\circ\text{C}$ , which is very close to the phase transition temperature we measured from thin films ( $413^\circ\text{C}$ ) [24]. Since the fabricated waveguides are not protected by a passivation layer, ChG layer deterioration and onset of sublimation at high temperature led to material loss, hence leading to a transmission power increase at higher temperatures ( $>500^\circ\text{C}$ ). For future devices, coating these chalcogenide films with a passivation layer will increase their oxidation and chemical resistance [26], thus enabling reliable and repeatable operation of these sensors.

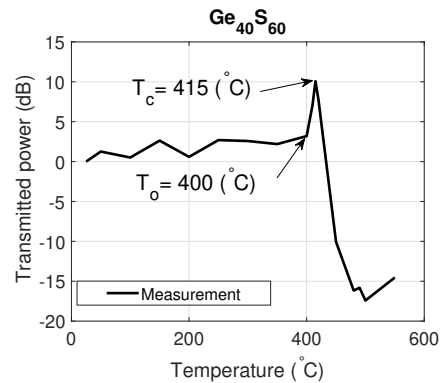


**Fig. 7.** Measured normalized transmitted power as a function of temperature with Ge<sub>40</sub>S<sub>60</sub> covered silicon waveguide-based temperature sensor.

Since the proposed temperature sensor works on principle of phase change of ChG material, which is highly temperature dependent, sudden changes in the transmitted power are observed, as expected. The slope as a function of temperature is plotted to extract the sudden change in the transmitted power as presented in Fig. 8.

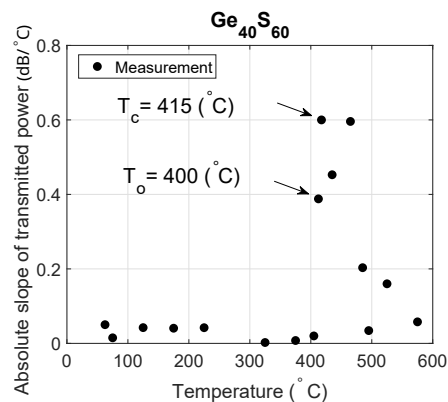


**Fig. 8.** Absolute slope of transmitted power as a function of temperature in temperature response of Ge<sub>40</sub>S<sub>60</sub> covered silicon waveguide based temperature sensor.

The sudden increase in the absolute slope of the transmitted power between T<sub>o</sub> and T<sub>c</sub> is due to large changes in structural reorganization occurring during the transition from the amorphous phase to the crystalline phases. The first crystallization peak is at T<sub>o</sub> = 400 °C and complete crystallization occurs at T<sub>c</sub> = 415 °C, which are experimentally recorded at 408 °C and 413 °C, respectively through monitoring the temperature of the heating stage [24]. The second highest peak is expected to be the second crystallization temperature of Ge<sub>40</sub>S<sub>60</sub> with T<sub>o2</sub> = 480 °C and T<sub>c2</sub> = 489 °C as shown in Table 1 in [24]. The second peak was not experimentally observed in our measurement. We believe that this is due to the specific structure which has developed in the thin films. Usually, DSC is measured on bulk materials in which the relaxation processes occur during heating. However, stress could be built into the films during the deposition process, thus preventing the relaxation-induced structure development for the second peak. Thus, this experiment confirms the functionality of the compact Si:ChG waveguide based temperature

sensor proposed in this work which help us with detection of real-time temperature inside a high temperature environment.

## 6. Reversibility

Reversibility is one of the most important properties of the device proposed in this work since this assures its application for multiple measurements. This was demonstrated on devices with electrodes in which electrical current can be applied after the device is cooled to room temperature. Application of current leads to Joule heating, which causes the crystalline chalcogenide material to melt. Next, a fast cooling step is performed to maintain equilibrium, characteristic for the liquid phase in the solidified product, i.e. to lock in the disorder within the material. This is indeed easy to achieve since the mass/volume of the melted film is negligible compared to the surrounding silicon substrate at room temperature, which assures fast cooling of the melted material.

Devices for reversibility demonstration were prepared by depositing aluminum electrodes on top of the chalcogenide glass layer, as shown in Fig. 9. After crystallization (SET), the devices were pulsed with a pulse generating unit (PGU) for 2 min with a square wave amplitude of 15V, a period of 7  $\mu$ s and an ON duration time of 50 ns. After pulsing, the transmitted power was measured again. It can be seen from Fig. 9 (green curve) that the transmitted power increases again. The RESET process enabled recovery of  $\sim 70\%$  of the device's initial transmitted power. We believe that the material degradation and partial sublimation during the crystallization process played a role in preventing 100% recovery of the power levels. Nevertheless, we successfully demonstrated reversible operation of the sensor.

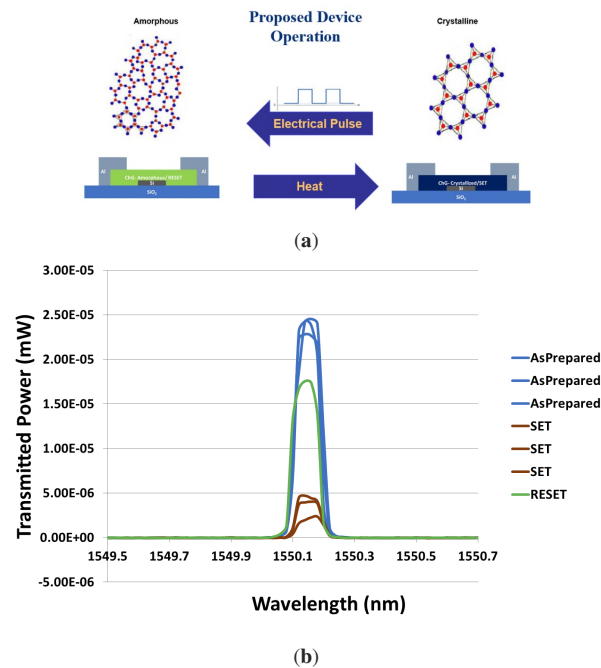


**Fig. 9.** (a) Cross section of a schematic of the waveguide device. (b) Transmitted power of the device in three states, Blue: Amorphous/As prepared, Red: Crystallized/SET and Green: Amorphized/ RESET.

## 7. Conclusions

A novel Si:ChG integrated waveguide sensor is demonstrated to be applicable for monitoring of temperature in extreme environments. The working principle of the sensor depends on the transformation of the glass from amorphous to crystalline phase at a specific crystallization temperature. According to the high loss of the ChG material in the crystalline phase compared to that in its amorphous phase, the Si:ChG waveguide exhibits a high extinction coefficient in the transmitted power. Therefore, by monitoring the output power from the waveguide as a function of temperature, the exact determination of the instant at which the reactor crosses the phase transition temperature can be achieved. The proposed Si:ChG based hybrid waveguide sensors for sensing cladding temperature of nuclear reactor are simulated using PhotonDesign software. The simulation data proved the optimum device dimensions which have been produced in this research on a SOI wafer. The Si waveguide design was patterned on an SOI wafer using EBL. We used the thermal evaporation method to cover the waveguide with a ChG synthesized by us. The measured temperature response of the fabricated sensor was in good agreement with the simulation results. The measured onset and crystalline temperatures are close to the values that we expected from studying the crystallization effects in the thin films. This remarkable property, together with CMOS-compatible fabrication of the silicon device and optical fibers promises a very reliable, low-cost, and reusable sensor network.

**Funding.** Nuclear Energy University Program (DE-NE008691).

**Acknowledgments.** This research was funded by U.S. Department of Energy's Office of Nuclear Energy created Nuclear Energy University Programs (NEUP) with grant number of DE-NE008691.

**Disclosures.** The authors declare no conflicts of interest.

**Data availability.** Data underlying the results presented in this paper are not publicly available at this time but may be obtained from the authors upon reasonable request.

## References

1. G. Locatelli, M. Mancini, and N. Todeschini, "Generation IV nuclear reactors: Current status and future prospects," *Energy Policy* **61**, 1503–1520 (2013).
2. B. Kallman, "The very high temperature reactor," Web, MAR (2013).
3. J. E. Kelly, "Generation IV international forum: A decade of progress through international cooperation," *Prog. Nucl. Energy* **77**, 240–246 (2014).
4. P. Pursula, I. Marttila, K. Nummila, and H. Seppä, "High frequency and ultrahigh frequency radio frequency identification passive sensor transponders for humidity and temperature measurement within building structures," *IEEE Trans. Instrum. Meas.* **62**(9), 2559–2566 (2013).
5. Y. Huang, Z. Zhou, Y. Zhang, G. Chen, and H. Xiao, "A temperature self-compensated LPFG sensor for large strain measurements at high temperature," *IEEE Trans. Instrum. Meas.* **59**(11), 2997–3004 (2010).
6. H. Hashemian, "Nuclear power plant instrumentation and control," *Nuclear Power–Control, Reliability and Human Factors*, InTech pp. 49–66 (2011).
7. F. Bucholtz and E. Udd, *Fiber optic magnetic sensors* (Wiley, 1991).
8. H. Golnabi, "Design and operation of a fiber optic sensor for liquid level detection," *Opt. Lasers Eng.* **41**(5), 801–812 (2004).
9. B. P. Pal, *Fundamentals of fibre optics in telecommunication and sensor systems* (Bohem press, 1992).
10. S. J. Mihailov, "Fiber bragg grating sensors for harsh environments," *Sensors* **12**(2), 1898–1918 (2012).
11. A. Kersey and T. Berkoff, "Fiber-optic bragg-grating differential-temperature sensor," *IEEE Photonics Technol. Lett.* **4**(10), 1183–1185 (1992).
12. H. Subbaraman, X. Xu, A. Hosseini, X. Zhang, Y. Zhang, D. Kwong, and R. T. Chen, "Recent advances in silicon-based passive and active optical interconnects," *Opt. Express* **23**(3), 2487–2511 (2015).
13. D. Adler, M. S. Shur, M. Silver, and S. R. Ovshinsky, *Threshold Switching in Chalcogenide-Glass Thin Films* (Springer US, Boston, MA, 1991).
14. T. Kavetsky, O. Shpotyuk, V. Balitska, G. Dovbeshko, I. Blonsky, I. Kaban, W. Hoyer, M. Iovu, and A. Andriesh, *Vibrational and structural properties of unmodified and radiation-modified chalcogenide glasses for advanced optical applications*, vol. 7142 (SPIE, 2008).
15. A. Barik, M. Bapna, D. Drabold, and K. Adarsh, "Ultrafast light induced unusually broad transient absorption in the sub-bandgap region of GeSe<sub>2</sub> thin film," *Sci. Rep.* **4**(1), 3686 (2015).
16. E. Udd and W. B. Spillman Jr, *Fiber optic sensors: an introduction for engineers and scientists* (John Wiley & Sons, 2011).

17. K. Grattan and T. Sun, "Fiber optic sensor technology: an overview," *Sens. Actuators, A* **82**(1-3), 40–61 (2000).
18. T. Wei, X. Lan, H. Xiao, Y. Han, and H.-L. Tsai, *Optical fiber sensors for high temperature harsh environment sensing* (2011).
19. A. Zakery and S. Elliott, "Optical properties and applications of chalcogenide glasses: a review," *J. Non-Cryst. Solids* **330**(1-3), 1–12 (2003).
20. K. Tanaka and K. Shimakawa, *Amorphous chalcogenide semiconductors and related materials* (Springer, 2011).
21. R. Wang, A. Rode, S. Madden, C. Zha, R. Jarvis, and B. Luther-Davies, "Structural relaxation and optical properties in amorphous Ge<sub>33</sub>As<sub>12</sub>Se<sub>55</sub> films," *J. Non-Cryst. Solids* **353**(8-10), 950–952 (2007). *Non-Crystalline Solids* 8.
22. A. Ahmadvand, B. Gerislioglu, R. Sinha, M. Karabiyik, and N. Pala, "Optical switching using transition from dipolar to charge transfer plasmon modes in Ge<sub>2</sub>Sb<sub>2</sub>Te<sub>5</sub> bridged metalodielectric dimers," *Sci. Rep.* **7**(1), 42807 (2017).
23. A.-A. Ahmed Simon, B. Badamchi, H. Subbaraman, Y. Sakaguchi, and M. Mitkova, "Phase change in Ge–Se chalcogenide glasses and its implications on optical temperature-sensing devices," *J. Mater. Sci.: Mater. Electron.* **31**(14), 11211–11226 (2020).
24. B. Badamchi, A.-A. A. Simon, M. Mitkova, and H. Subbaraman, "Chalcogenide glass-capped fiber-optic sensor for real-time temperature monitoring in extreme environments," *Sensors* **21**(5), 1616 (2021).
25. S. Pathak, *Photonics integrated circuits* (Elsevier, 2019).
26. M. Kumar, S. Rani, A. Kumar, J. Tawale, R. Srivastava, B. P. Singh, S. Pathak, X. Wang, and V. Singh, "Broadband (NIR-Vis-UV) photoresponse of annealed SnSe films and effective oxidation passivation using Si protective layer," *Mater. Res. Bull.* **153**, 111913 (2022).